

Benzocyclobutene Polymer as an Additive for a Benzocyclobutene-Fullerene: Application in Stable p-i-n Perovskite Solar Cells

Marie-Hélène Tremblay^a, Kelly Schutt^b, Federico Pulvirenti^a, Thorsten Schultz^{c, d}, Berthold Wegner^{c, d}, Xiaojia Jia^d, Yadong Zhang^a, Elena Longhi^a, Raghunath R. Dasari^a, Canek Fuentes Hernandez^d, Bernard Kippelen^d, Norbert Koch^{c, d}, Henry J. Snaith^b, Stephen Barlow^a, Seth R. Marder^{a*}

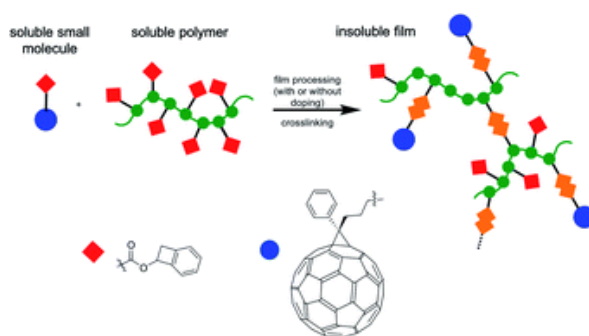
^a School of Chemistry and Biochemistry, and Center for Organic Photonics and Electronics (COPE), Georgia Institute of Technology, Atlanta, GA, 30332, United States

^b Clarendon Laboratory, Department of Physics, University of Oxford, Oxford, OX1 3PU, United Kingdom

^c Humboldt-Universität zu Berlin, Institut für Physik & IRIS Adlershof, Berlin, 12489, Germany

^d Helmholtz-Zentrum für Materialien und Energie GmbH, Berlin, 12489, Germany

^e School of Electrical and Computer Engineering, and Center for Organic Photonics and Electronics (COPE), Georgia Institute of Technology, Atlanta, GA, 30332, United States



Abstract

A poly(methacrylate) with benzocyclobutene side chains, CL, has been synthesized by radical polymerization for use as a crosslinking additive for a previously reported benzocyclobutene-functionalized fullerene, PCBCB, which can be thermally insolubilized following solution processing. Films of PCBCB incorporating CL and n-doped with $(\text{IrCp}^*\text{Cp})_2$ exhibit in-plane electrical conductivities around ten times higher than those of n-doped films without CL, while the use of CL also reduces leaching of dopant ions from the film upon washing. The performance and stability of perovskite solar cells using insolubilized PCBCB:CL, insolubilized PCBCB, or PCBM as top electron-extraction layers are compared; cells with undoped PCBCB:CL extraction layers exhibit higher average and maximum power conversion efficiencies (16 and 18.5%, respectively) than their PCBM and PCBCB counterparts. Devices with undoped PCBCB:CL extraction layers also showed excellent thermal stability, retaining 92% of their stabilized power output after aging for 3000 h at 85 °C in the dark in a nitrogen atmosphere.

Introduction

Hybrid organic–inorganic perovskites have been extensively studied as the absorber layer in solar cells due to their high absorption in the visible spectrum, tunable band gap, and long carrier diffusion length.^{1–7} Despite their impressive performance, lead halide perovskite solar cells (PSCs) still require further advancement in terms of long-term stability. The diffusion of dopant ions, halide ions and metal ions originating from the electrodes are all known to be significant degradation pathways.^{8–11}

Electron-transport materials (ETM) play a crucial role in PSCs by reducing the charge recombination that occurs at direct perovskite/electron-collecting electrode interfaces. Fullerene derivatives work well and have been extensively used in PSCs, in part due to the favorable alignment of their lowest unoccupied molecular orbitals with the conduction band of perovskite absorbers. Insolubilization of the ETM subsequent to deposition is an effective approach to increase the mechanical and thermal stability of the material, to permit solution deposition of additional layers, and may also be expected to restrict diffusion of ions.¹² Several such approaches have been reported to the insolubilization of ETMs in perovskite solar cells, including thermal removal of solubilizing imide substituents from a naphthalene diimide,¹³ thiol–ene crosslinking chemistry involving hexaazatrinaphthalene ETM moieties,¹⁴ and hydrolysis of a fullerene sol–gel precursor.¹⁵ Some of the authors of the present paper reported an analogue of the widely used PCBM (Fig. 1) in which the methyl group is replaced by a benzocyclobutene (BCB) moiety: [6,6]-phenyl-C₆₁-butyric acid 1- benzocyclobutenyl ester (PCBCB). Heating to 190–200 °C results in the formation of fullerene oligomers (PCBCB)_n (dimers are detected by mass spectrometry) and insolubilization of films in solvents such as DMF and chlorobenzene.^{15,16} BCBs are well known to undergo thermal ring opening of the four-membered ring to give *o*-quinodimethane derivatives, which can then dimerize to form dibenzocyclooctanes. In PCBCB the quinodimethane intermediates can also undergo cycloaddition with the fullerene core (see Fig. S1†).^{16,17} We have previously used thermally insolubilized (PCBCB)_n to prevent aggregation of fullerenes in OPVs under thermal aging at 150 °C,¹⁶ and as an ETM in so-called n–i–p (negative–intrinsic–positive) PSCs,¹⁵ which reached stabilized power conversion efficiencies (PCEs) above 17%.¹⁸

We speculate that the stability of PCBCB films might be further improved if fully crosslinked films could be formed on heating. Here we report the synthesis and characterization of a crosslinker, CL (Fig. 1), consisting of poly(methacrylate) with pendant BCB groups, as an approach to increasing connectivity between the (PCBCB)_n oligomers. The effect of the n-dopant (IrCp*₂)₂ (Fig. 1) and CL additions on PCBCB and on the performance and stability of positive–intrinsic–negative (p–i–n) PSCs with PCBCB ETLs are studied and discussed.

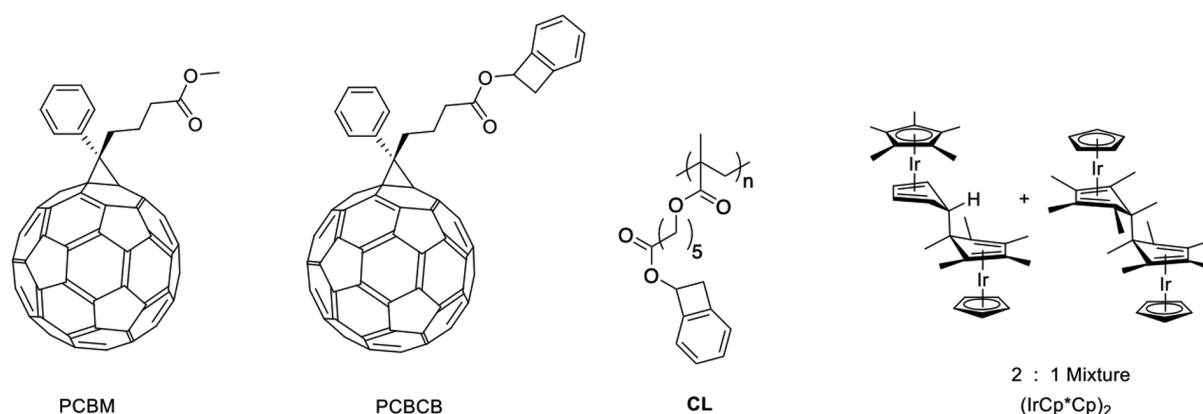


Fig. 1. Molecular structures of the molecules studied here: the ETMs PCBM (reference) and PCBCB, the crosslinker (CL) and the *n*-type electrical dopant (IrCp* Cp)₂.

Results and discussion

Synthesis and characterization of a new ETM system

PCBCB and (IrCp* Cp)₂ were synthesized as reported previously.^{15,19} The polymeric crosslinker CL was synthesized *via* polymerization of a methacrylate monomer containing a BCB moiety using the radical initiator azobisisobutyronitrile (AIBN) (see Fig. 2). The polymer had good solubility in chlorobenzene, the solvent used in previous work for the solution deposition of PCBCB. Gel permeation chromatography against polystyrene standards yielded a molecular weight of 580 kg mol⁻¹ and a dispersity index of 2 (see Fig. S3[†]). BCB esters of the type incorporated in PCBCB and CL typically undergo ring-opening at *ca.* 200 °C; indeed, we have previously used differential scanning calorimetry to study PCBCB thermal properties and shown that a broad exothermic peak is observed with an onset of *ca.* 150 °C and a peak maximum at *ca.* 210 °C in the first scan, but that this feature is completely absent in subsequent scans, indicating quantitative ring-opening of the BCB units,¹⁶ while heating for 10 min at 190–200 °C was shown to insolubilize PCBCB in a variety of solvents (likely indicating that even dimers of this molecule are insoluble).¹⁵ Heating of the PCBCB:CL blends to 200 °C for 10 min results in similarly insoluble films.

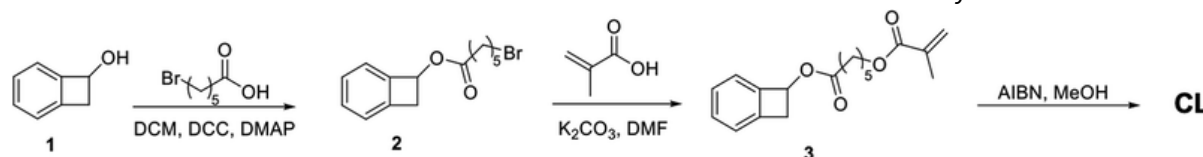


Fig. 2. Synthesis of the crosslinker CL. DCM = dichloromethane, DCC = *N,N'*-dicyclohexylcarbodiimide, DMAP = 4-dimethylaminopyridine, DMF = *N,N*-dimethylformamide, AIBN = azobisisobutyronitrile, MeOH = methanol.

n-Doping can be used to fill electronic traps and increase the number of charge carriers in an ETM, leading to increased conductivity of the ETM, and to reduce barriers for electron extraction (and injection). Moderately air-stable 19-electron sandwich organometallic dimers, (MCp* Cp)₂ (where Cp* = pentamethylcyclopentadienyl; Cp = cyclopentadienyl, M = Rh,²⁰ Ir¹⁹) and (RuCp* mes)₂,²¹ can *n*-dope ETMs with electron affinities as small as *ca.* 2.8 eV and do not form byproducts.^{22–26} The fairly large size of the corresponding monomeric cations formed on doping, at least relative to those of species such as alkali-metal ions, may hinder their diffusion in the ETM layer. (IrCp* Cp)₂ can dope both solutions of PCBCB (see Fig. S2[†]) and films of (PCBCB)_{*n*} (see Fig. S4[†]), forming fullerene radical anions, PCBCB^{•-}, and

iridium monomer cations, $(\text{IrCp}^*\text{Cp})^+$. As the molar concentration of dopant is increased, the absorption peak corresponding to the neutral acceptor at 330 nm¹⁶ decreases in intensity while the presence of a peak at 1070 nm, corresponding to the fullerene radical anion,^{27,28} becomes more evident (see Fig. S2†). UPS shows how the ionization energy ($\text{IE} = \phi + \text{VBO}$, where ϕ is the work function and VBO is the valence band onset) of $(\text{PCBCB})_n$ films on FTO decreases by up to 0.6 eV with increasing addition of $(\text{IrCp}^*\text{Cp})_2$, suggesting that the number of occupied states increases (see Fig. S3†).

Transmission-line measurements were performed to quantify the impact of dopant and cross-linker addition on the in-plane electrical conductivity of $(\text{PCBCB})_n$ films. The sheet resistance (R_s) of the ETMs spin-coated on glass with a silver electrode on top was measured to determine their conductivity (σ), their resistivity (ρ), and the resistance at the ETM/Ag contact (R_c) (see Fig. S4 and Tables S1 and S2†).

A $(\text{PCBCB})_n$ film insolubilized by heating to 200 °C for 10 min has an in-plane conductivity comparable to that of PCBM films. When the organometallic dimer is incorporated into the casting solution, the conductivity of $(\text{PCBCB})_n$ increases by up to four orders-of-magnitude ($3.7 \times 10^{-7} \pm 2.2 \times 10^{-7} \text{ S cm}^{-1}$ to $1.4 \times 10^{-3} \pm 3.8 \times 10^{-4} \text{ S cm}^{-1}$), confirming doping of the ETM by the Ir-dimer (see Fig. S4 and Table S1†). To assess the impact of the introduction of CL (1–30 mol%) on the in-plane electrical conductivity, the nominal concentration of $(\text{IrCp}^*\text{Cp})^+$ in the $(\text{PCBCB})_n$ films (based on the contents of the casting solution) was kept constant at 3 mol%. Use of 1 mol% CL in the casting solution causes the conductivity to increase ten-fold ($3.3 \times 10^{-4} \pm 2.3 \times 10^{-4} \text{ S cm}^{-1}$ to $5.5 \times 10^{-3} \pm 5.4 \times 10^{-4} \text{ S cm}^{-1}$). The conductivity remains roughly constant with additional CL, up to 30 mol% ($5.9 \times 10^{-3} \pm 3.4 \times 10^{-3} \text{ S cm}^{-1}$). This may be related to previous observations that the rheological, mechanical and electrical properties of organic semiconductors can in some cases be improved by addition of simple polymers such as poly(methyl methacrylate (PMMA) (*i.e.*, a polymer similar to CL, but lacking the BCP side chain).^{29–34}

We performed X-ray photoelectron spectroscopy measurements (XPS) to determine the impact of CL addition on the retention of $(\text{IrCp}^*\text{Cp})^+$ cation in $(\text{PCBCB})_n$ films upon washing (see Fig. 3). We measured the elemental composition of $(\text{PCBCB})_n$ films (doped with a nominal 3 mol% of IrCp^*Cp) with and without crosslinker, as prepared and after spin-coating solvents commonly used in device fabrication (chlorobenzene and DMF). Without CL, the iridium elemental contribution – calculated from the area under the Ir 4f peaks – of the $(\text{PCBCB})_n$ films decreases upon washing with chlorobenzene and DMF. When 10 mol% of CL was added in the precursor solution of doped PCBCB, the elemental contribution of iridium remains unchanged after washing with DMF or chlorobenzene, showing a better immobilization of the dopant in the films containing CL.

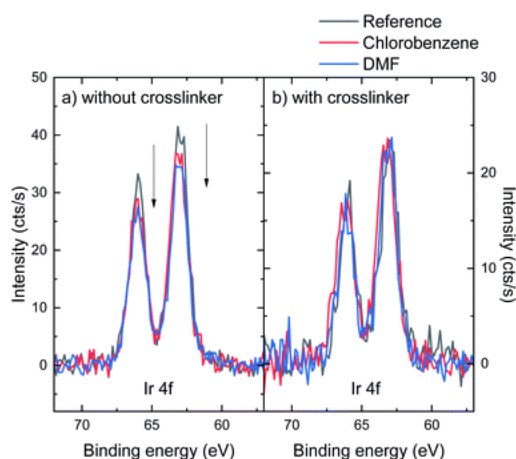


Fig. 3. Iridium elemental contribution in doped $(\text{PCBCB})_n$ films with 3 mol% $(\text{IrCp}^*\text{Cp})_2$ without CL (a) and with 10 mol% CL (b) as prepared, and after spin-coating chlorobenzene or DMF onto the film. The elemental contribution of iridium is calculated from the area under the Ir 4f peaks in XPS spectra. The carbon elemental contribution in the same films is constant regardless of washing.

Perovskite solar cells fabrication and characterization

PSCs with the p–i–n architecture were fabricated to assess the impact of the additive crosslinker on device performance and stability. The device structure was FTO/ F_4 -TCNQ-doped PolyTPD/ $\text{Cs}_{0.05}(\text{FA}_{0.85}\text{MA}_{0.15})_{0.95}\text{Pb}(\text{I}_{0.9}\text{Br}_{0.1})_3/\text{ETM}/\text{BCP}/\text{Ag}$, where ETM is either PCBM or $(\text{PCBCB})_n$ with and without crosslinker and dopant, FA is formamidinium, MA is methylammonium, polyTPD is poly(4-butyl-triphenylamine-4',4''-diyl) and BCP is bathocuproine. The selected perovskite is a relatively stable triple cation (FAMACs) lead mixed-halide perovskite, processed from solutions of DMF and dimethylsulfoxide (DMSO). State-of-the-art solar cells with ETM = PCBM were used as the reference. The device performance parameters averaged over 20 solar cells for each type of ETM, as well as the champion cells, are shown in Table 1 (see Fig. S6, S7 and Tables S3 and S4† for optimization of CL concentration and dopant concentration). The current density–voltage (J – V) curves of the best-performing solar cells are shown in Fig. 4. We note that the J – V curves exhibit fairly pronounced hysteresis: we have previously found that the hysteresis seen in solar cells using this triple-cation perovskite is dependent on the interface between the perovskite and the charge-collection layers.³⁵ Accordingly, we also show plots of the steady-state power output and current density in Fig. 4B.

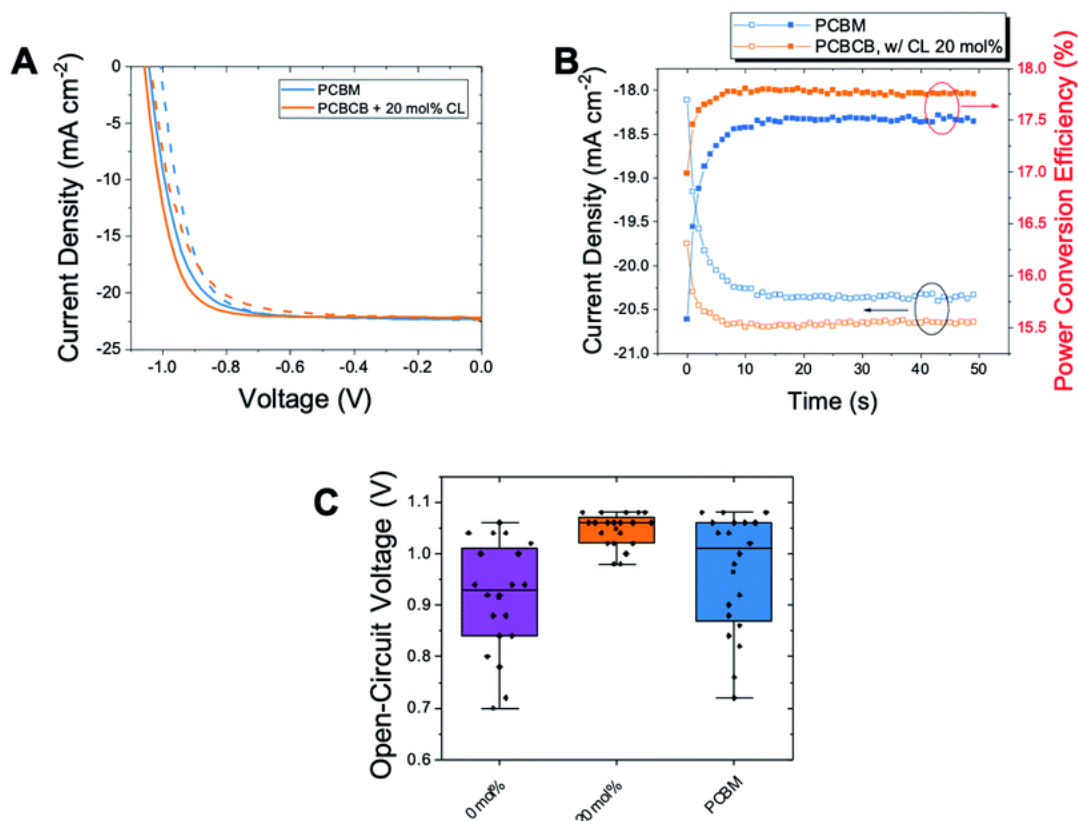


Fig. 4. (A) J - V characteristics for champion devices employing $(\text{PCBCB})_n$ with 20 mol% CL and PCBCB collected under AM 1.5G simulated sunlight. Solid line: reverse scan, dotted line: forward scan. (B) Steady-state power output and current density over time. (C) Comparison of V_{oc} for $(\text{PCBCB})_n$, $(\text{PCBCB})_n$ with 20 mol% CL and PCBM.

Table 1. Statistics for 20 individual FAMACs devices using undoped ETM. PCBCB films were thermally insolubilized

| | | J_{sc} (mA cm ⁻²) | V_{oc} (V) | FF | PCE (%) |
|---------------------------------------|---------|------------------------------------|-----------------|-------------|------------|
| $(\text{PCBCB})_n$ | Average | 21 ± 2 | 0.92 ± 0.1 | 0.65 ± 0.05 | 12 ± 2 |
| | Maximum | 23.20 | 1.06 | 0.72 | 15.35 |
| $(\text{PCBCB})_n$ with 20 mol% CL | Average | 21.5 ± 0.8 | 1.05 ± 0.03 | 0.68 ± 0.03 | 16 ± 2 |
| | Maximum | 22.87 | 1.08 | 0.78 | 18.54 |
| PCBM | Average | 20 ± 2 | 1.0 ± 0.1 | 0.70 ± 0.07 | 14 ± 3 |
| | Maximum | 22.39 | 1.08 | 0.77 | 17.64 |

On average, the V_{oc} values obtained during the reverse scan are 0.92 V and 1.05 V for PSCs fabricated with undoped $(\text{PCBCB})_n$ and $(\text{PCBCB})_n\text{-CL}$, respectively. The increase in V_{oc} , shown in Fig. 4, suggests a reduction of non-radiative recombination at the interface. Moreover, variations in V_{oc} across devices with $(\text{PCBCB})_n\text{-CL}$ (20 + mol%) are smaller compared to those in devices with unmodified $(\text{PCBCB})_n$, $(\text{PCBCB})_n\text{-CL}$ with lower cross-linker content, or PCBM, showing better reproducibility of the devices incorporating CL in the ETL (see also Fig. S7†); this decreased spread in V_{oc} values with increased CL content is reproducible from batch to batch and suggests that the presence of a high CL content leads to a more consistent perovskite:ETL contact, perhaps by more consistently passivating the perovskite surface. The improved average V_{oc} for $(\text{PCBCB})_n\text{-CL}$ PSCs leads to an

improvement of PCE, which is 16% on average, with a maximum value of 18.5%. The champion cells containing (PCBCB)_n-CL exceeded the performance of those using state-of-the-art PCBM as ETM.

While doping PCBM with n-dopants such as *N*-DMBI-H improves the performance of the PSC using this architecture,^{36–40} those made with (IrCp**Cp*)₂-doped (PCBCB)_n did not show an improvement over the undoped analogue (see Fig. S6 and Table S3†). Nevertheless, in other types of architecture, this type of dopant has been seen to improve the performance of the PSCs.^{24,25,41} The *V*_{oc} of the PSCs decreases upon doping of the ETM, perhaps due to increased charge recombination at the perovskite:ETM interface. It has previously been shown that improvements in the conductivity of a charge-transport material do not necessarily lead to an improvement of the solar cell performance,^{42,43} likely when, as here, the extraction layer is relatively thin.

The photoluminescence (PL) properties of the different ETMs on top of the perovskite film on glass are comparable, which is not surprising due to the chemical similarities of the ETMs. The carrier lifetime and photoluminescence quantum efficiency (PLQE) are similar across all ETMs. Notably, the PL spectra appear to contain two features: one centered at ~770 nm and one at ~790 nm. Since this material contains mixed halides, we presume that the higher energy feature corresponds to the majority phase emission of Cs_{0.05}(FA_{0.85}MA_{0.15})_{0.95}Pb(I_{0.9}Br_{0.1})₃ and the lower energy feature corresponds to iodide-rich phase-segregated domains.^{44,45} Since we observe a smaller contribution from the low-energy emission feature from all the films containing the ETM layers, our results suggest that the halide segregation is suppressed by the presence of the ETM layers, possibly due to a lower net photoinduced electron density in the perovskite absorber layer due to electron extraction (Fig. 5).

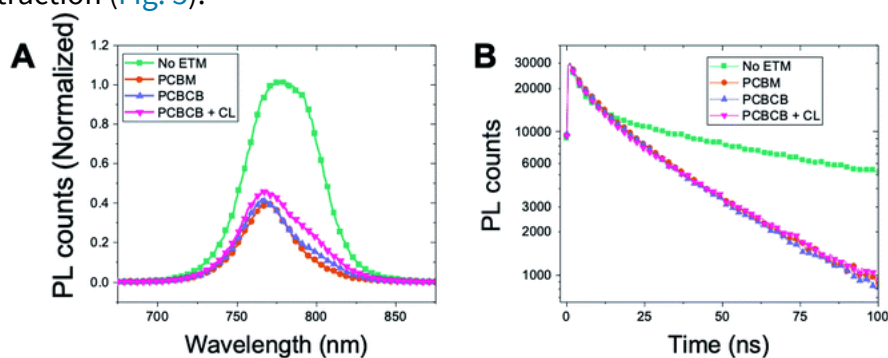


Fig.5. Steady state PL (A) and time-resolved PL (B) of half devices on FTO.

Stability of perovskite solar cells

PSCs with the p–i–n architecture were aged in the dark in inert atmosphere at 85 °C to investigate the dependence of the thermal stability on the choice of ETM (see Fig. 6 for doped ETM and Fig. S8† for undoped analogue). PSCs fabricated from the same batch were brought to atmosphere and room temperature for steady-state power output (SPO) measurement. Despite some initial fluctuations, the PSCs were stable for more than 3000 h. In both cases, doped and undoped cells, the additive cross-linker ((PCBCB)_n-CL) appears to improve the stability of the cells over the PCBM reference. Notably, after 3000 hours, the best (PCBCB)_n-CL cells retained 99% of their 950 h efficiency (92% of initial efficiency), while the PCBM ones retained 89% (82% of initial efficiency).

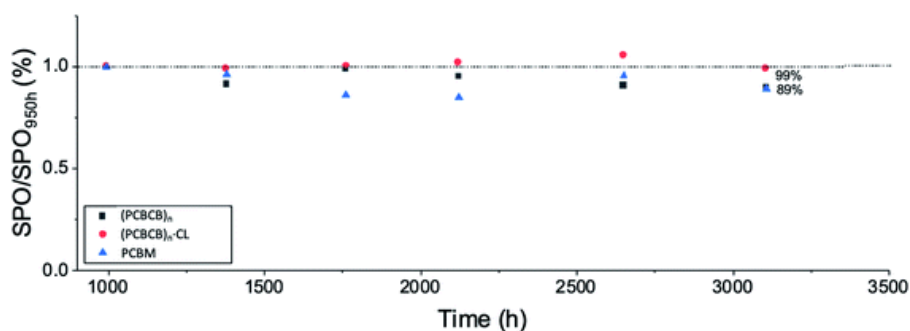


Fig. 6. Stability comparison of non-encapsulated PSCs, stressed at 85 °C in the dark in a N₂ atmosphere, fabricated using undoped (PCBCB)_n, (PCBCB)_n-CL (20 mol%) and PCBM. An average of four devices per each data point is reported. The SPO is normalized with the SPO after the initial improvement of the PSCs.

Conclusions

Here we report the effect of adding a polymeric crosslinking additive, CL, to thermally insolubilize fullerene PCBCB in p-i-n PSCs. We demonstrated that (IrCp* Cp)₂ can electrically dope a fullerene derivative and that doped insoluble films of (PCBCB)_n oligomers exhibit four orders-of-magnitude higher in-plane electrical conductivity than the undoped material. Adding an additive crosslinker, CL, inhibits washing of (IrCp* Cp)⁺ from the film and does not negatively affect the electrical conductivity of the doped (PCBCB)_n.

While the conductivity of the (PCBCB)_n film was improved using the (IrCp* Cp)₂ dopant, the performance of the PSCs decreased with its addition. PSCs made using (PCBCB)_n with CL leads to an improvement in PCE, as well as an improved performance reproducibility. The PSC degradation is diminished compared to PCBM reference, showing a promising avenue to obtain long-term stable solar cells.

Acknowledgement

This work was supported by NSERC (ES. D. Scholarship for MHT), the AFOSR (FA9550-15-0115 and FA9550-18-1-0499), the NSF (DMR-1729737), the Marshall Aid Commemoration Commission, EPSRC UK, the National Nuclear Security Administration through the Consortium for Nonproliferation Enabling Technologies (DE-NA0002576), the Department of Energy/National Nuclear Security Administration (DE-NA0003921), and the Deutsche Forschungsgemeinschaft (DFG) (423749265 – SPP 2196). We thank Khaled Al Kurdi and Felipe Larrain for useful discussions on electrical conductivity, and David McMeekin for training and discussions.

References

1. R. J. Sutton, G. E. Eperon, L. Miranda, E. S. Parrott, B. A. Kamino, J. B. Patel, M. T. Hörantner, M. B. Johnston, A. A. Haghighirad, D. T. Moore and H. J. Snaith, *Adv. Energy Mater.*, 2016, **6**, 1502458.
2. G. E. Eperon, S. D. Stranks, C. Menelaou, M. B. Johnston, L. M. Herz and H. J. Snaith, *Energ. Environ. Sci.*, 2014, **7**, 982-988.
3. G. Xing, N. Mathews, S. Sun, S. S. Lim, Y. M. Lam, M. Grätzel, S. Mhaisalkar and T. C. Sum, *Science*, 2013, **342**, 344-347.

4. S. D. Stranks, G. E. Eperon, G. Grancini, C. Menelaou, M. J. P. Alcocer, T. Leijtens, L. M. Herz, A. Petrozza and H. J. Snaith, *Science*, 2013, **342**, 341-344.
5. Q. Dong, Y. Fang, Y. Shao, P. Mulligan, J. Qiu, L. Cao and J. Huang, *Science*, 2015, **347**, 967-970.
6. A. Kojima, K. Teshima, Y. Shirai and T. Miyasaka, *J. Am. Chem. Soc.*, 2009, **131**, 6050-6051.
7. M. M. Lee, J. Teuscher, T. Miyasaka, T. N. Murakami and H. J. Snaith, *Science*, 2012, **338**, 643
8. C. Bi, Q. Wang, Y. Shao, Y. Yuan, Z. Xiao and J. Huang, *Nat. Comm.*, 2015, **6**, 7747.
9. C. Eames, J. M. Frost, P. R. F. Barnes, B. C. O'Regan, A. Walsh and M. S. Islam, *Nat. Comm.*, 2015, **6**, 7497.
10. Y. Kato, L. K. Ono, M. V. Lee, S. Wang, S. R. Raga and Y. Qi, *Adv. Mater. Interfaces*, 2015, **2**, 1500195.
11. G. Zhang, S. A. Hawks, C. Ngo, L. T. Schelhas, D. T. Scholes, H. Kang, J. C. Aguirre, S. H. Tolbert and B. J. Schwartz, *ACS Appl. Mater. Interfaces*, 2015, **7**, 25247-25258.
12. L. Derue, O. Dautel, A. Tournebize, M. Drees, H. Pan, S. Berthumeyrie, B. Pavageau, E. Cloutet, S. Chambon, L. Hirsch, A. Rivaton, P. Hudhomme, A. Facchetti and G. Wantz, *Adv. Mater.*, 2014, **26**, 5831-5838.
13. T. Nakamura, N. Shioya, T. Shimoaka, R. Nishikubo, T. Hasegawa, A. Saeki, Y. Murata, R. Murdey and A. Wakamiya, *Chem. Mater.*, 2019, **31**, 1729-1737.
14. Z. Zhu, D. Zhao, C.-C. Chueh, X. Shi, Z. Li and A. K. Y. Jen, *Joule*, 2018, **2**, 168-183
15. K. Wojciechowski, I. Ramirez, T. Gorisse, O. Dautel, R. Dasari, N. Sakai, J. M. Hardigree, S. Song, S. Marder, M. Riede, G. Wantz and H. J. Snaith, *ACS Energy Lett.*, 2016, **1**, 648-653.
16. N. Deb, R. R. Dasari, K. Moudgil, J. L. Hernandez, S. R. Marder, Y. Sun, A. Karim and D. G. Bucknall, *J. Mater. Chem. A*, 2015, **3**, 21856-21863.
17. A. Gügel, P. Belik, M. Walter, A. Kraus, E. Harth, M. Wagner, J. Spickermann and K. Müllen, *Tetrahedron*, 1996, **52**, 5007-5014.
18. D. P. McMeekin, Z. Wang, W. Rehman, F. Pulvirenti, J. B. Patel, N. K. Noel, M. B. Johnston, S. R. Marder, L. M. Herz and H. J. Snaith, *Adv. Mater.*, 2017, **29**, 1607039.
19. O. V. Gusev, M. G. Peterleitner, M. A. Ievlev, A. M. Kal'sin, P. V. Petrovskii, L. I. Denisovich and N. A. Ustynyuk, *J. Organomet. Chem*, 1997, **531**, 95-100.
20. O. V. Gusev, L. I. Denisovich, M. G. Peterleitner, A. Z. Rubezhov, N. A. Ustynyuk and P. M. Maitlis, *J. Organomet. Chem*, 1993, **452**, 219-222.
21. O. V. Gusev, M. A. Ievlev, M. G. Peterleitner, S. M. Peregudova, L. I. Denisovich, P. V. Petrovskii and N. A. Ustynyuk, *J. Organomet. Chem.*, 1997, **534**, 57-66
22. S. K. Mohapatra, A. Fonari, C. Risko, K. Yesudas, K. Moudgil, J. H. Delcamp, T. V. Timofeeva, J.-L. Brédas, S. R. Marder and S. Barlow, *Chem.: Eur. J.*, 2014, **20**, 15385-15394.

23. S. Olthof, S. Mehraeen, S. K. Mohapatra, S. Barlow, V. Coropceanu, J.-L. Brédas, S. R. Marder and A. Kahn, *Phys. Rev. Lett.*, 2012, **109**, 176601.
24. F. Pulvirenti, B. Wegner, N. K. Noel, G. Mazzotta, R. Hill, J. B. Patel, L. M. Herz, M. B. Johnston, M. K. Riede, H. J. Snaith, N. Koch, S. Barlow and S. R. Marder, *Mol. Syst. Des. & Eng.*, 2018, **3**, 741-747.
25. J. Avila, M.-G. La-Placa, E. Longhi, M. Sessolo, S. Barlow, S. R. Marder and H. J. Bolink, *J. Mater. Chem. A*, 2019, **7**, 25796-25801.
26. S. Guo, S. B. Kim, S. K. Mohapatra, Y. Qi, T. Sajoto, A. Kahn, S. R. Marder and S. Barlow, *Adv. Mater.*, 2012, **24**, 699-703
27. D. V. Konarev, N. V. Drichko and A. Graja, *J. Chim. Phys.*, 1998, **95**, 2143-2156.
28. B. D. Naab, S. Guo, S. Olthof, E. G. B. Evans, P. Wei, G. L. Millhauser, A. Kahn, S. Barlow, S. R. Marder and Z. Bao, *J. Am. Chem. Soc.*, 2013, **135**, 15018-15025.
29. G. Lu, H. Tang, Y. Qu, L. Li and X. Yang, *Macromolecules*, 2007, **40**, 6579-6584.
30. F. S. Kim and S. A. Jenekhe, *Macromolecules*, 2012, **45**, 7514-7519.
31. J. Sun, B. J. Jung, T. Lee, L. Berger, J. Huang, Y. Liu, D. H. Reich and H. E. Katz, *ACS Appl. Mater. Interfaces*, 2009, **1**, 412-419.
32. Y. Kubota and Y. Tominaga, *Mater. Today Commun.*, 2015, **4**, 124-129.
33. G. Lu, L. Bu, S. Li and X. Yang, *Adv. Mater.*, 2014, **26**, 2359-2364.
34. L. Qiu, W. H. Lee, X. Wang, J. S. Kim, J. A. Lim, D. Kwak, S. Lee and K. Cho, *Adv. Mater.*, 2009, **21**, 1349-1353.
35. H. J. Snaith, A. Abate, J. M. Ball, G. E. Eperon, T. Leijtens, N. K. Noel, S. D. Stranks, J. T.-W. Wang, K. Wojciechowski and W. Zhang, *J. Phys. Chem. Lett.*, 2014, **5**, 1511-1515
36. Z. Bin, J. Li, L. Wang and L. Duan, *Energ. Environ. Sci.*, 2016, **9**, 3424-3428.
37. S. S. Kim, S. Bae and W. H. Jo, *Chem. Comm.*, 2015, **51**, 17413-17416.
38. G. Kakavelakis, T. Maksudov, D. Konios, I. Paradisanos, G. Kioseoglou, E. Stratakis and E. Kymakis, *Adv. Energy Mater.*, 2017, **7**, 1602120.
39. C. Kuang, G. Tang, T. Jiu, H. Yang, H. Liu, B. Li, W. Luo, X. Li, W. Zhang, F. Lu, J. Fang and Y. Li, *Nano Lett.*, 2015, **15**, 2756-2762.
40. Z. Yang, J. Xie, V. Arivazhagan, K. Xiao, Y. Qiang, K. Huang, M. Hu, C. Cui, X. Yu and D. Yang, *Nano Energy*, 2017, **40**, 345-351.
41. F. Pulvirenti *Doctoral dissertation*, Georgia Institute of Technology, 2019
42. A. Pellaroque, N. K. Noel, S. N. Habisreutinger, Y. Zhang, S. Barlow, S. R. Marder and H. J. Snaith, *ACS Energy Lett.*, 2017, **2**, 2044-2050.

43. M.-H. Tremblay, K. Schutt, Y. Zhang, J. Lim, Y.-H. Lin, J. H. Warby, S. Barlow, H. J. Snaith and S. R. Marder, *Sustain. Energy Fuels*, 2020, **4**, 190-198.
44. E. T. Hoke , D. J. Slotcavage , E. R. Dohner , A. R. Bowring , H. I. Karunadasa and M. D. McGehee , *Chem. Sci.*, 2015, **6** , 613-617.
45. S. Mahesh , J. M. Ball , R. D. J. Oliver , D. P. McMeekin , P. K. Nayak , M. B. Johnston and H. J. Snaith , *Energy Environ. Sci.*, 2020, **13** , 258-267.